Small-amplitude magnetization dynamics in permalloy elements investigated by time-resolved wide-field Kerr microscopy

Andreas Neudert,* Jeffrey McCord,† Dmitry Chumakov, Rudolf Schäfer, and Ludwig Schultz
Leibniz Institute for Solid State and Materials Research IFW Dresden, Institute for Metallic Materials, Helmholtzstrasse 20, D-01069 Dresden, Germany

(Received 28 May 2004; revised manuscript received 26 October 2004; published 11 April 2005; corrected 18 April 2005)

A wide-field polarization microscope, optimized for Kerr microscopy was extended with a mode-locked pulsed laser illumination source to investigate time-dependent magnetization processes with picosecond resolution, thus providing the possibility to directly compare the quasistatic with the dynamic magnetization response. Square-shaped $Ni_{81}Fe_{19}$ elements were excited by fast magnetic field pulses aligned along and diagonally to the elements, respectively. Starting from the Landau ground state, the magnetic response to the excitation is dominated by a fast rotation of magnetization followed by slow relaxation, mostly through domain wall motion, back into the Landau state. Spike domains in the corners of the element form during the fast rotational process. Low angle domains with oscillatory behavior develop in the low dynamic permeability closure domains. Slow motion of the center vortex over several nanoseconds is recorded. The direct comparison of the dynamic and the static domain patterns is necessary for a understanding of all details of the magnetization processes.

DOI: 10.1103/PhysRevB.71.134405 PACS number(s): 75.60.−d

I. INTRODUCTION

The understanding and control of fast magnetization reversal processes is critical for applications in data storage and spin electronics. First systematic experiments on permalloy using an inductive method were already performed around 1960.[1,2] A better insight on the mechanisms of the magnetization processes can be gained from dynamic domain imaging. In 1963 Conger and Moore[3] reported on an optical stroboscopic method to investigate the high-speed magnetization reversal in magnetic $Ni_{80}Fe_{20}$ films. They used sunlight and a mirror fastened to a turbine spinning at 10^6 rpm to produce light pulses of about 100 ns duration. With the development of pulsed low repetition ns-pulse width laser technology different types of experimental setups evolved. These systems were used for the investigation of magnetic bubble dynamics,[4,5] and later for studies on excited recording write heads.[6–10] Two fundamental methods, scanning and wide-field microscopy, were applied. In contrast to wide-field Kerr microscopy (where an image of a certain area is gained immediately), scanning microscopy probes the magnetization only at a small surface area with a focused laser beam. By scanning the sample under the microscope objective an image of the magnetic microstructure can be extracted.

A breakthrough in terms of time resolution is related to the development of ps- and fs-laser systems. The first scanning Kerr microscope with a time resolution in the ps regime was reported by Freeman and Smyth[11] for the investigation of magnetic flux propagation in recording head pole tips. This method is now well established and widely used for investigations in magnetic thin films and recording heads.[12–17] Other experiments using scanning Kerr microscopy focus onto the eigenmodes of the magnetization in magnetic elements[18] and the gyrotropic motion of a central vortex in magnetic thin film elements.[19] In addition to the magneto-optical methods other time-resolved imaging techniques, namely, time-resolved x-ray photoemission electron microscopy (XPEEM) and magnetic transmission x-ray microscopy (MTXM) demonstrated great potential[20–25] and were used for similar studies. An overview over different methods for magnetic imaging can be found in Refs. 26–28. Most of the experiments so far were restricted to small elements below 10 μm in dimension.

In this article we report on time-resolved wide-field magneto-optical microscopy with ps time resolution and its application to investigations of fast magnetization processes in extended ferromagnetic thin film elements. The focus of this article is to study the change of the magnetic ground states with low-field excitations. We restrict our studies to permalloy thin film elements due to its excellent soft magnetic properties and low uniaxial anisotropy.

II. EXPERIMENT

We extended a standard optical wide-field polarization microscope that was optimized for Kerr microscopy with a mode-locked solid-state Nd:YVO_4 laser, which produces 12-ps wide laser pulses at a fixed repetition rate of 23 MHz (see Fig. 1). The wavelength of the laser pulses is shifted from 1064 nm (infrared) to 532 nm (green) by frequency doubling. A continuous adjustment of illuminating power is achieved by rotating the polarization axis of the infrared laser light using an integrated $\lambda/2$ wave plate before frequency doubling. The output power can be set to any value between zero and approximately 500 mW. The visible output, in our case, is reduced to less than 150 mW matching with the sensitivity range of the detection CCD camera. By using a multimode glass fiber (2 m in length, core diameter 200 μm), the laser light is fed into the microscope, replacing the standard light source of the microscope. The image of the fiber output is focused to a small spot in the back focal plane

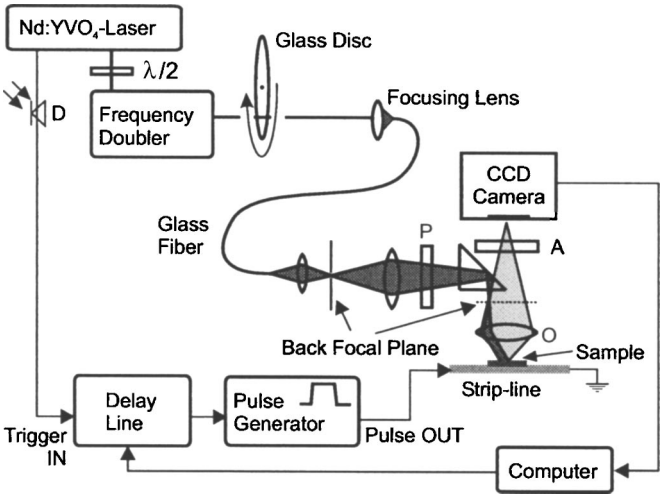

FIG. 1. Experimental setup consisting of laser, polarization microscope (schematically shown by a prism, lenses, microscope objective *O*, polarizer *P*, and analyzer *A*), CCD camera, pulse generator, delay generator, strip line, and the sample. The delay generator and consecutively the pulse generator is triggered by a photo diode (*D*). The image is transferred to a computer where it is further processed.

of the objective. This ensures an almost parallel illumination of the sample. Sensitivity to in-plane magnetization by means of the longitudinal Kerr effect is achieved by placing the fiber output off centered to the optical axis, resulting in oblique incidence of light. The sensitivity axis is parallel to the plane of incidence. By moving the off-centered fiber output around the optical axis in the back focal plane of the objective, the plane of incidence and the sensitivity axis is adjusted. A more detailed description of Kerr microscopy and the alignment of the optical path can be found in Ref. 26.

Due to the coherence of the laser, speckle patterns disturb the image of the sample. To avoid the interfering speckles, the laser beam is sent through a roughened spinning glass plate. The glass plate moves the interference pattern during the integration time of the CCD camera, so that an in average homogeneously illuminated image is obtained. A similar scheme was used in Ref. 29 for a cw laser (continuous wave) illumination.

The exposure time for each frame of the CCD camera used in our experiments is typically 50 ms. During that time more than 10^6 laser pulses reach the sample in phase with the high speed magnetic field excitation. This stroboscopic way of imaging limits our investigations to repetitive magnetization processes. To enhance the contrast, a background image, containing all the nonmagnetic information, is subtracted from the raw image. To acquire the background image the sample preferable is saturated with an external dc magnetic field. After subtracting the saturated background image, the difference image contains only information about the spatial magnetization distribution. Alternatively, the background image is acquired without magnetic field (i.e., at delay positions before the pulsed magnetic field arrives). By using this method the *change* of the spatial magnetization pattern with respect to the magnetic ground state is visualized. To improve the signal-to-noise ratio, up to 20 raw and background images are acquired and accumulated for each measurement.

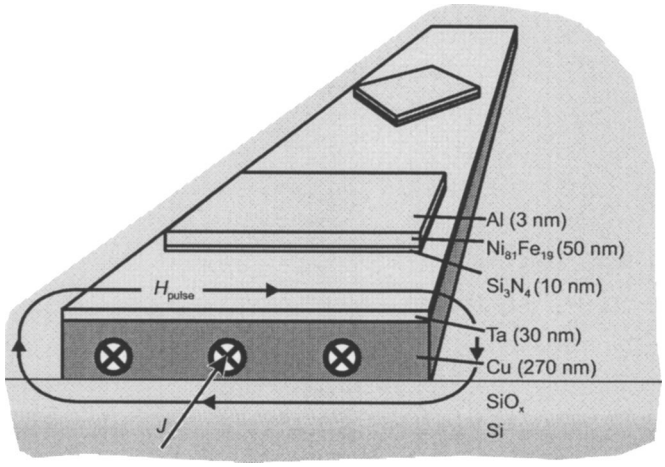

FIG. 2. Sketch of the center conductor of the coplanar waveguide with the permalloy elements on top. The direction of the generated magnetic field H_{pulse} is indicated. The size of the square element is 40×40 μm^2 for the aligned and 28×28 μm^2 for the tilted element, respectively. The element length along the field direction is the same.

The pulsed magnetic field is produced by guiding voltage pulses through a 50-μm-wide impedance matched ($Z=50\ \Omega$) coplanar waveguide. Depending on the used high-speed voltage sources, pulses with 20/80 rise times down to 125 ps and amplitudes of up to 13 V can be achieved. The calibration procedure to obtain the amplitude of the pulsed magnetic field is described in Ref. 30. The pulse generator is triggered by the signal of a photodiode that is illuminated by the infrared laser light. The trigger signal is shifted with respect to the laser pulse by using an electric delay line. As the delay line is operating by means of an electrical relay, the minimal step of the delay is fixed at 25 ps, given by the minimal used cable lengths. No additional electrical jitter is added by this scheme, in contrast to other electrical delay setups.[28] Experimentally we obtain a time resolution of approximately 20 ps. The laser's fixed repetition rate of 23 MHz limits our observation time slot to approximately 43 ns.

In Fig. 2 a sketch of the coplanar waveguide together with the permalloy elements is shown. The waveguide consists of a Cu layer covered by a thin Ta layer to obtain similar optical properties for the strip-line surface and the magnetic elements. An insulating Si_3N_4 layer was added in between the strip line and the magnetic film to electrically insulate the magnetic elements. The strip lines were structured by optical lithography and a consequent chemical wet-etch process. The 50-nm-thin permalloy film was deposited without an external magnetic field by dc-magnetron sputtering on top of the central conductor. An additional Al cover layer was added for corrosion protection. The magnetic elements were formed in a photoresist layer by standard optical lithography and etched by ion milling.

III. RESULTS

A. Parallel-aligned square element

In general, the quasistatic magnetization process in small fields is dominated by domain wall displacement as demon-

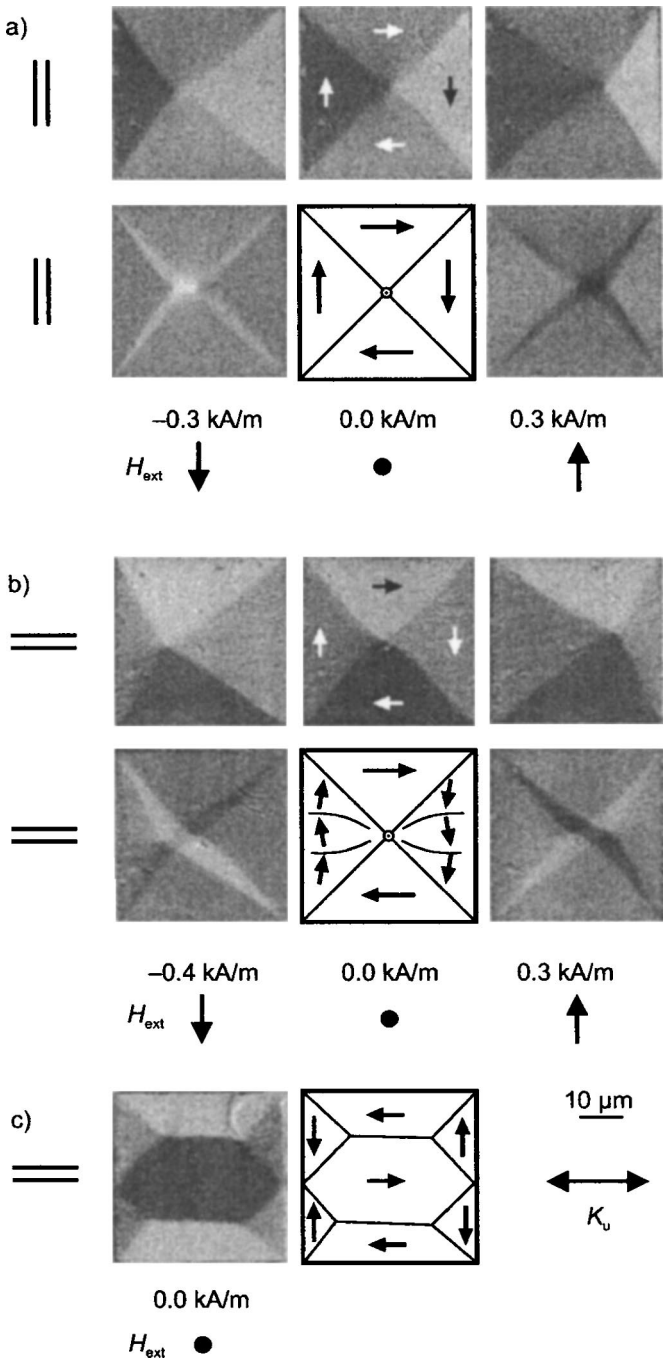

FIG. 3. (a) Vortex (⊙) movement in a slowly changing magnetic field. The magneto-optical sensitivity is aligned vertically (‖). The direction and amplitude of the field H_{ext} is indicated. The images of the upper row display the magnetization distribution of the Landau state, whereas in the second row the change of magnetization relative to the Landau state is shown. The images in (b) are taken at approximately the same field values but the sensitivity axis (as indicated) is oriented perpendicular relative to (a). A seven-domain state with a horizontal orientation of 180° domain walls is displayed in (c), indicating the presence of a uniaxial anisotropy K_u.

strated in Fig. 3. The response of the vortex ground state of the aligned square permalloy element to a slowly changing magnetic field for two orthogonal sensitivity axes is shown. The domains with a magnetization component parallel to the external field have a lower energy than those with an antiparallel component. The motion of the domain walls (domain wall displacement) leads to a minimization of the total energy by growing of the domains with parallel magnetization components at the expense of the domains with antiparallel aligned magnetization components.

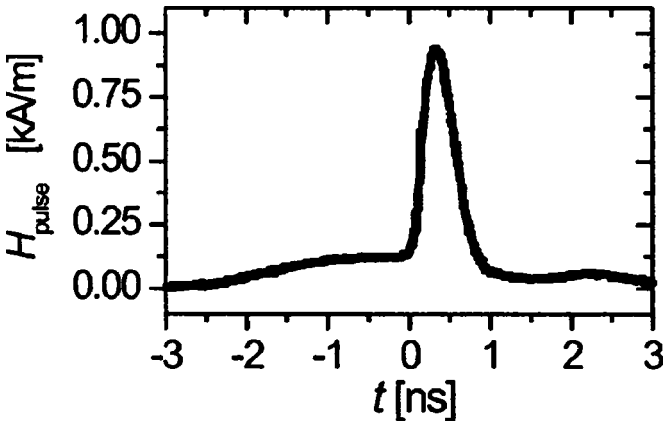

FIG. 4. Magnetic field pulse, derived from the voltage pulse measured with an oscilloscope. The rise- and fall-time (20/80) of the pulse is about 160 and 300 ps, respectively. The pulse width is 450 ps (FWHM). The pulse repetition rate is 23 MHz.

Another important detail is visible in Fig. 3(b). The magnetization in the left and right domains is not homogeneous, but rather slightly modulated as indicated schematically. Due to the contribution of a horizontally aligned uniaxial anisotropy, the energy in the Landau state gets minimized by the development of additional small angle domain walls inside the hard-axis closure domains. The modulation also reflects itself in an undulation of the 90° domain walls. The presence of the uniaxial anisotropy becomes obvious from Fig. 3(c), where a seven-domain state in the same element is shown. This domain state is obtained by saturating the sample along the vertical edge and decreasing the amplitude of the magnetic field. The 180° walls in the seven-domain state are aligned parallel to the uniaxial anisotropy. By applying the field along the horizontal axis (i.e., parallel to the uniaxial anisotropy) and decreasing its amplitude the four-domain vortex state develops. Note that in permalloy elements of this size several different metastable states may appear after reducing the magnetic field. In some rare cases we also observed the formation of a "tulip" structure[26] at a corner of the square. The control and understanding of the initial magnetic states is rather important and the base for the understanding of the dynamic magnetization behavior.

The dynamic reversal processes are very different compared to the quasistatic case. The characteristics of the fast excitation field are shown in Fig. 4. The direction of the pulsed field in these dynamic experiments is the same as the direction of the external field in the quasistatic experiments of Fig. 3. The dynamic response of the element is shown in Fig. 5. A qualitative representation of the magnetization distribution as derived from the Kerr images is sketched at the right.

The magnetization processes can be described as follows. The initial magnetization in the upper and lower domains is

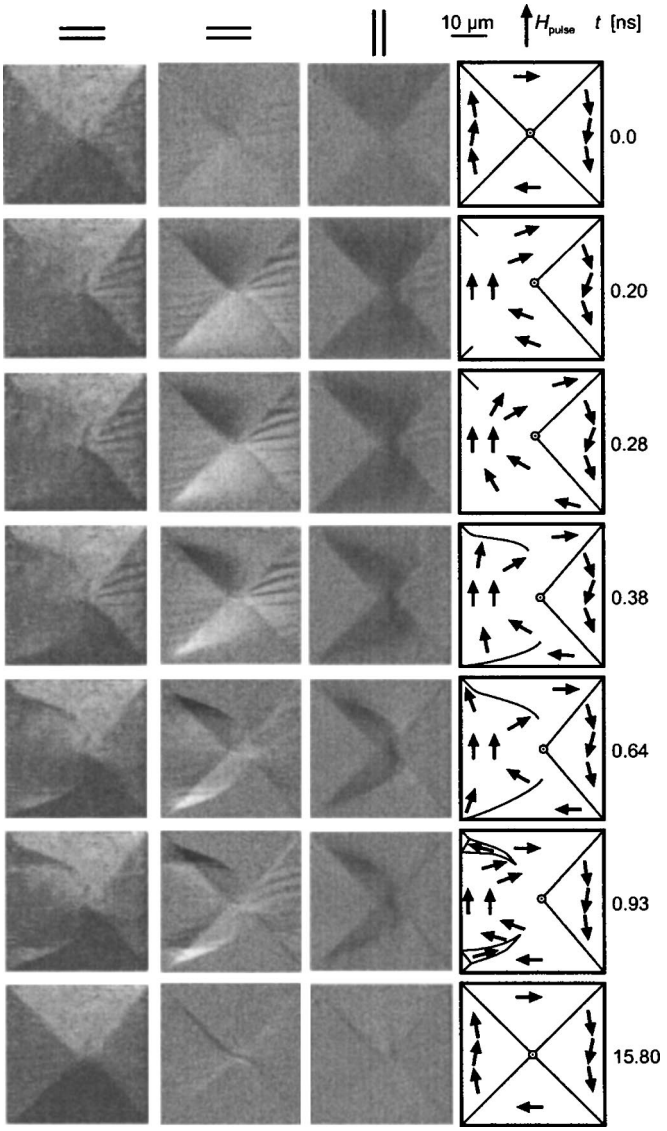

FIG. 5. Dynamic magnetization response of the Landau state of the 40×40 μm^2 square element. The applied field characteristics is shown in Fig. 4. The left column represents the magnetic microstructure with the sensitivity axis perpendicular to the magnetic field pulse. The two center columns display the change of the magnetization with respect to the Landau state. Both orthogonal sensitivity axes are shown. The right column shows the magnetization vectors as derived qualitatively from the Kerr images. The center vortex position (⊙) is indicated.

oriented perpendicular to H_{pulse}, which results in a maximum of torque $\vec{M}\times\vec{H}_{\text{eff}}$ on the magnetization. This torque forces the magnetization to rotate around the axis of the effective field that includes also the demagnetizing field. Due to the influence of the demagnetizing field the magnetization located in the center of the element is rotated to a larger degree than the magnetization near the edges of the element. This can be recognized best in the left image at $t=0.28$ ns, where the contrast near the center of the element is equal to that of the vertically aligned left domain, meaning that the magnetization is aligned completely upward along the direction of H_{pulse}. In contrast, the magnetization near the horizontally

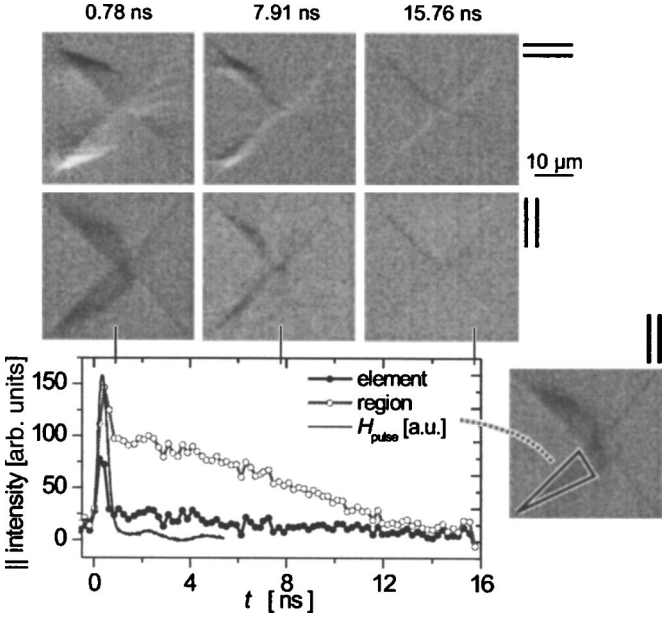

FIG. 6. Change of magneto-optical signal in time integrated over the complete element and of a small region for longitudinal sensitivity, respectively. The plot shows the in-plane intensity *parallel* to H_{pulse}. Exemplary difference images for both orthogonal sensitivity directions are shown.

aligned edges, which are aligned perpendicular to the applied magnetic field, remains almost unchanged in all images. Due to the rotation of magnetization in the upper and lower domains, the two initial 90° walls from the center to the upper and lower left corners are almost completely dissolved. Only the 90° walls inside the far corners of the element reside. The vortex structure is broadened to a width of several micrometer. As the magnetization at the edges remains concurrently unchanged, between the top and bottom edge of the element the magnetization has to rotate by 180° for topological reasons. At $t=0.64$ ns two spike domains develop at the upper and lower left corners. These spike domains develop by a clock and counterclockwise rotation of magnetization at the bottom and top of the element, respectively. The formation of these spike domains reduces the magnetostatic energy that increases due to the rotation of magnetization in the center of the element. Thus they act similar to the 90° walls in the field-free initial Landau state. No domain wall movement is involved in the evolution of the new domain pattern. Note the similarity between the corner domains and the initial concertina domains visible in magnetic elements during quasistatic reversal.[30,31] Finally, the magnetization relaxes back into the Landau state and the spike domains dissolve slowly (within about 15 ns), but now by domain wall movement. This process is rather slow compared to the almost instantaneous formation of the spike domains that is completed after approximately 0.6 ns.

The relaxation process is best quantified by comparison of the integrated Kerr signal for the longitudinal sensitivity direction. The change of magnetization with time for the entire element and for a selected region are plotted together with the pulse profile in Fig. 6. The change of the magneto-optical signal for the complete element and therefore the overall

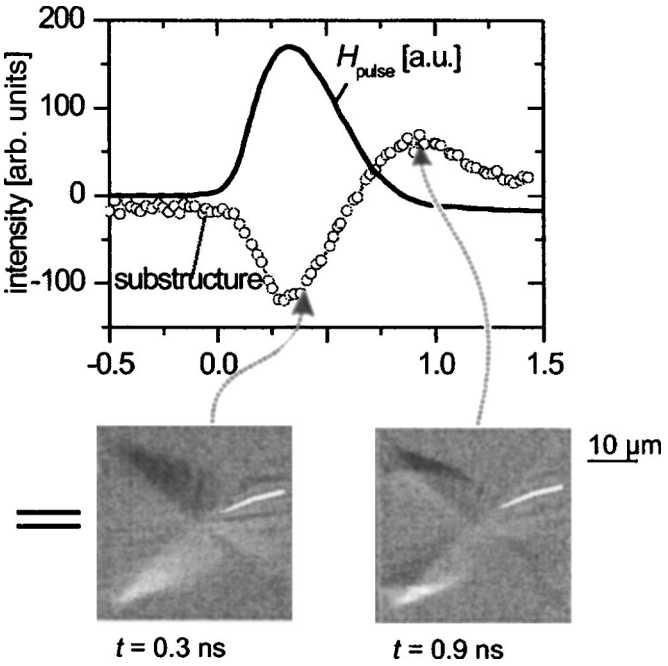

FIG. 7. Oscillating Kerr intensity of a small region (indicated by the white area) within the domain with the modulated magnetization distribution versus time. At $t \approx 0.7$ ns the contrast in this pattern changes its sign and at $t = 0.90$ ns the inversion is at its maximum.

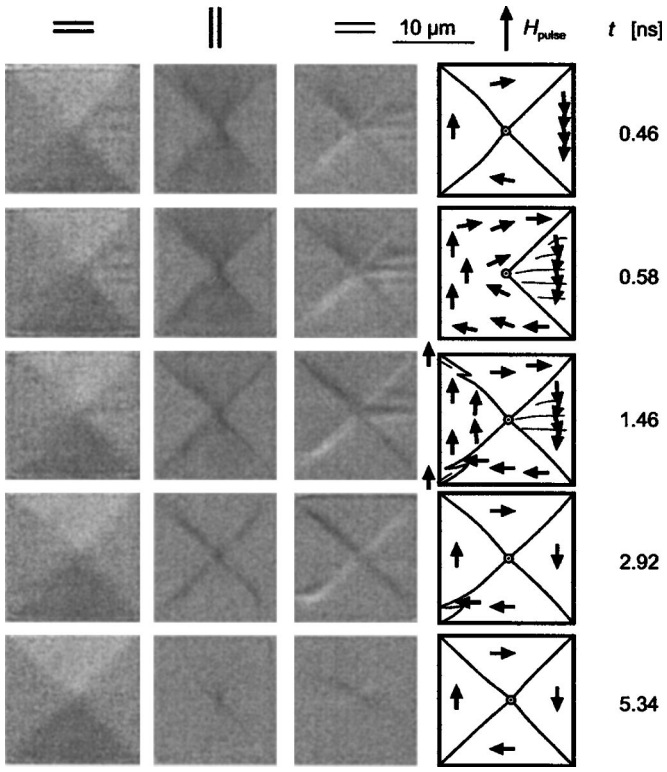

FIG. 8. Dynamics of the Landau state in a 16×16 μm^2 square element. Due to the smaller size of the element we increased the pulsed field amplitude to about 1500 A/m. This value was obtained by comparing the initial susceptibilities of the magneto-optically measured hysteresis loops of the two elements.

magnetization follows the time evolution of H_{pulse}. Obviously, the element's magnetization as a whole is able to instantaneously follow the magnetic field within the pulse. The local magnetization distribution, however, changes over time. This is best demonstrated by integrating the magnetization response over the triangular area, where domain wall motion occurs (indicated in the images on the right in Fig. 6). Again, the plot displays a peak at the onset of the applied pulse field. However, as H_{pulse} drops back to zero a magnetization component aligned along the formerly applied magnetic field remains. This magnetization component degrades slowly. The relaxation process is completed after 15 ns as derived from the intensity plot (see also domain formation in Fig. 5).

Another detail becomes visible in Fig. 5. Aligning the Kerr sensitivity axis perpendicular to H_{pulse}, a ripplelike modulation of magnetization inside the domain with an antiparallel alignment between $\vec{M}$ and $\vec{H}_{pulse}$ is seen. This pattern does not change its basic structure with elapsing time. However, the horizontal magnetization component reverses at $t \approx 0.7$ ns, which becomes apparent in the analysis of the change of magneto-optical signal inside one of the small-angle domains (Fig. 7). Note that the initial background Kerr image [see also Fig. 3(b)], taken at zero field, already possesses a modulated substructure inside both hard-axis domains. Due to the contrary alignment of H_{pulse} and magnetization in the right domain, the deviation of local magnetization from the mean direction is intensified in this domain and the pattern gets clearly visible in the dynamic images. At the reversal the pulsed magnetic field is almost zero again and the magnetization rotates back into its equilibrium position with a slight undershoot. The ringing of magnetization leads to a inversion of contrast in the ripple domains (see also Fig. 5).

During the whole reversal process the center vortex almost stays in its original position. Whereas the 90° walls at the left dissolve (Fig. 5), the two Néel walls on the right side of the element remain almost unchanged, which indicates that the vortex is still in the center of the element. After the relaxation process at about 15.8 ns the vortex structure is almost restored. Only a weak domain signal in the center and of the surrounding 90° walls is visible in the difference images. In Ref. 32 micromagnetic calculations of the response of permalloy elements similar to our experiments are performed. The initial magnetic microstructure at the ground state is the same as in our investigation. The main difference to our experiments is the size of the elements, being much smaller than in our case (about 1 μm edge length). As the element's dimension is quite different to our investigations, only a qualitative comparison can be given here. However, one similarity between this simulation and the experimental data presented here is the lower mobility of the vortex compared to the mobility of the surrounding domain walls.

The low mobility of the center vortex is also visible in the images of a 16×16 μm^2 square element shown in Fig. 8. As in the larger element, the modulation of the magnetization antiparallel to H_{pulse} is enhanced. The development of spike domains is also visible for the smaller element. However, due to the stronger influence of the pinned 90° walls in the

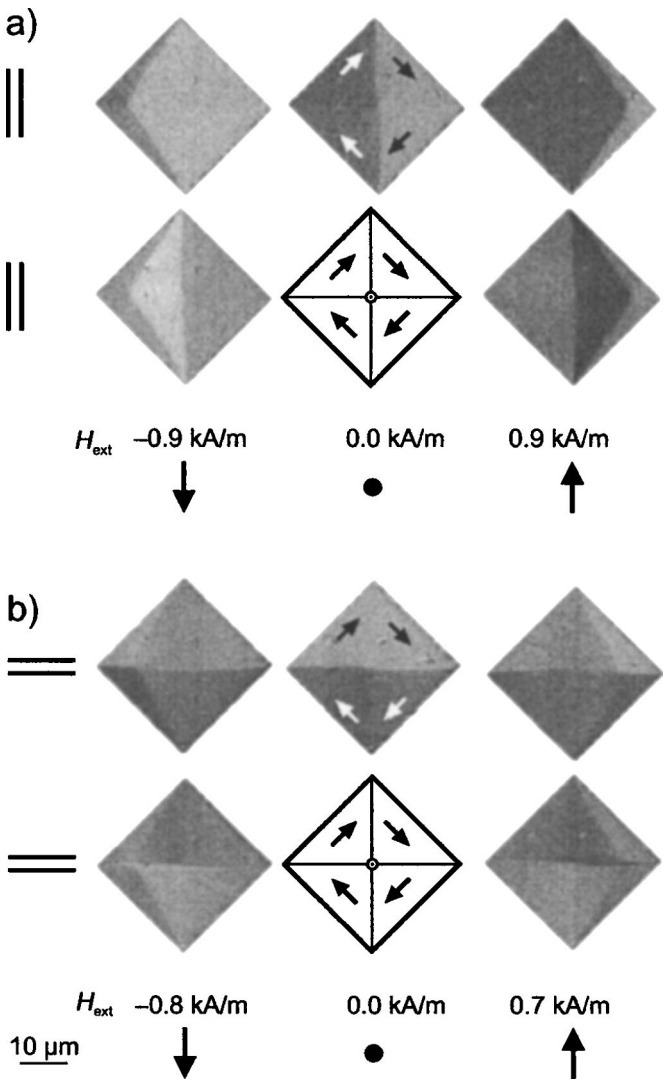

FIG. 9. Quasistatic vortex movement in the tilted square. The sensitivity axes and methods for background subtraction are the same as in Fig. 3.

corners of the element, the spike domains are less pronounced and resolve faster than in the case of the $40 \times 40\ \mu m^2$ element. The spike domain in the top corner is almost not existent and dissolves much faster than the domain in the lower left corner. Only a weak change of magnetization relative to the initial state is visible after 5 ns, mostly in the region of the low mobility vortex structure.

B. Tilted square element

As the dynamic magnetization behavior of the domain network is strongly determined by the high-frequency permeability of the domains surrounding the central vortex, we investigated the response of the Landau state in a tilted square element of $28 \times 28\ \mu m^2$ size for comparison. One major difference to the experiments shown before is that all four domains exhibit a noticeable $\vec{M} \times \vec{H}_{pulse}$ torque, a fast rotation of magnetization is expected in all domains. The response to quasistatic excitation is seen in Fig. 9. In contrast to Sec. III A, the magnetic field is applied parallel to the element diagonal. The quasistatic response of the element follows the same rules as for the other element (Fig. 3). The domains with a parallel component of magnetization relative to the applied field grow at the expense of the domains with an antiparallel component. Due to this domain wall displacement the vortex position is shifted to the left or to the right, depending on field direction and vortex rotational direction.

The dynamic response to the same pulsed field (Fig. 4) is shown in Fig. 10. As mentioned above, due to the diagonal direction of H_{pulse} a torque now applies to the magnetization in all four domains. This becomes apparent by the immediate response of all four domains to the exciting field pulse visible by the simultaneous change of magneto-optical contrast in both images at $t=0.23$ ns in Fig. 10. As for the nontilted element, spike domains are generated. They appear at $t=0.33$ ns at the top and bottom corner. Note that the magnetization in these domain is aligned opposite to the applied field direction. The magnetization near the left edge of the element rotates back into its orientation parallel to the edge and a curved wall is formed on the left side of the element ($t=0.52$ ns). Again, as for the parallel oriented element investigated before, no domain wall motion is involved in this process. With increasing time, the spike domains grow and merge with the bended domain wall ($t=0.75$–0.95 ns). This process is relatively fast and completed within 1 ns. However, at this point a depinning of the vortex and the main domain wall structure occurs. The vertical wall itself is shifted to the right, but the vortex remains slightly displaced to the left relative to the bended wall (visible at $t=0.95$ ns). The displacement of vortex core and domain wall lasts for approximately 0.8 ns (not shown). The subsequent relaxation process is dominated by slow vortex movement, with the 90° walls being now pinned to the vortex core. As a consequence the domain walls, capable of moving faster than the vortex, become bended, but oppositely to the state after $t \approx 0.5$ ns. The relaxation back into the Landau state is not even completed after 15 ns as can be seen from the images in the bottom row of Fig. 10. No ripple domains are observed in the case of the tilted element.

For comparison, in another experiment we excited the same element with a continuous pulse train of 5.4 ns wide pulses switching from −400 to +400 A/m. The magnetization dynamics of the excitation with fast switching alternating fields is shown in Fig. 11. The pulse shape is displayed in Fig. 11(b). The main difference to the previous experiments is that a magnetic field is acting on the sample now during most of the time. Therefore no relaxation of the domain pattern in zero field state occurs. As before, we observe spike domains in the top and bottom corners of the element. As the field keeps applied in time, no immediate relaxation occurs. With the rotation of magnetization in the domains with an antiparallel component of magnetization relative to H_{pulse}, the spike domains develop. Congruently with the evolution of two off-centered 90° walls the spike domains dissolve almost completely. The wall connects the two corners of the element. Note that the magnetization pattern at $t=4.89$ ns is just opposite to the initial domain pattern at $t=-0.09$ ns, before the onset of field reversal.

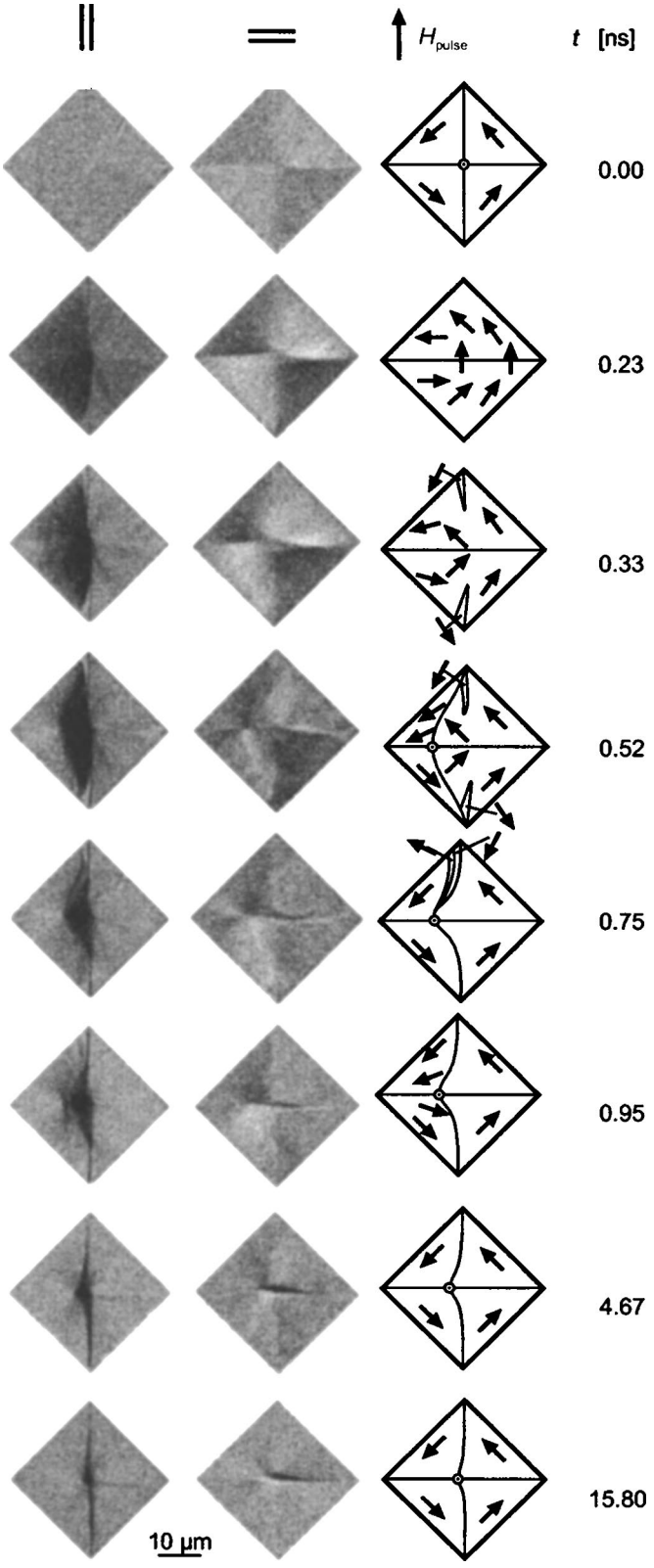

FIG. 10. Response of the Landau state of the 28×28 μm^2 tilted square element to the pulsed magnetic field. The left and middle column represent the change of the magnetization with respect to the Landau state at two different sensitivity axes (see also Fig. 5). The magnetization vectors in the right column are qualitatively estimated from the Kerr images. The vertex position is indicated.

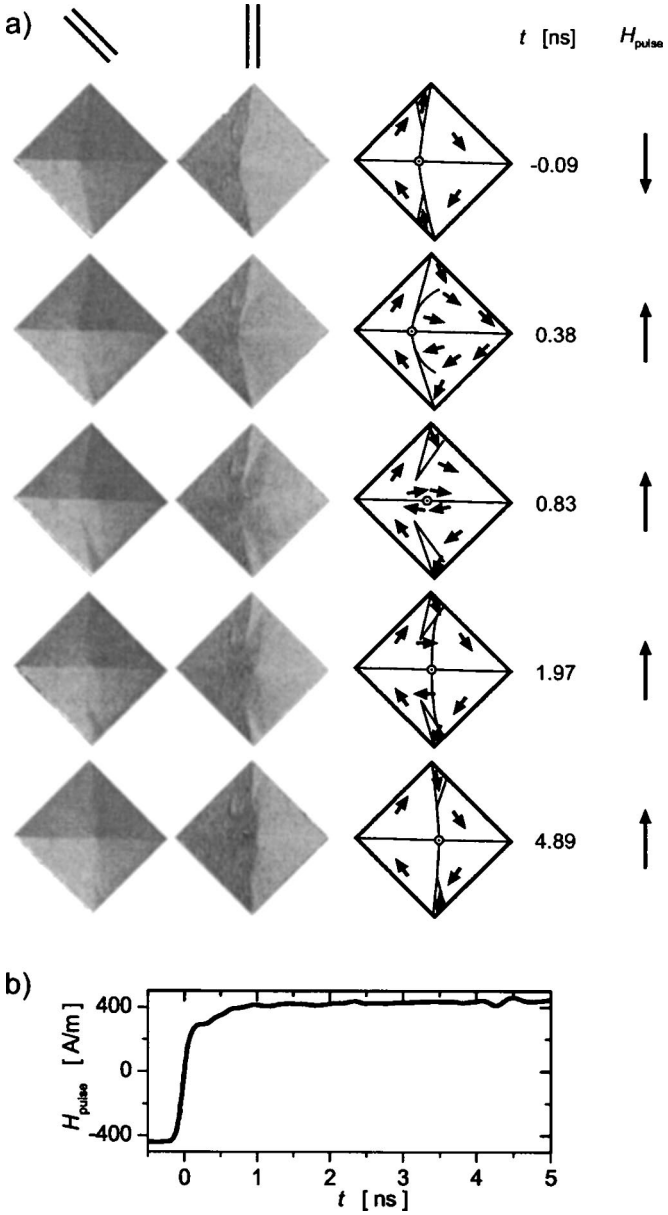

FIG. 11. (a) Response of the Landau state of the tilted element to the pulsed magnetic field shown in (b) (5.4 ns pulse width).

C. Discussion

The formation of the spike domains at the corners in both element geometries (Figs. 5 and 10) indicates that this formation is independent of the direction of the pulsed field with respect to the edges of the square. In both cases the magnetization near the corners rotates contrary to H_{pulse} to partly compensate the demagnetizing field originating from the rotation of magnetization in the center of the element. Due to this rotation spike domains are generated. These domains relax rather slowly in the parallel aligned square element, whereas in the case of the tilted element they merge with the surrounding domains (see images at $t=0.52$ ns and at $t=0.75$ ns in Fig. 10). The reason for the difference is related to the lower mobility of the formed 180° walls (Fig. 5) as shown in our data. Due to the effective torque acting on

all domains, the 90° walls move faster in the case of the tilted element (Fig. 10). The images shown in Fig. 11 reveal that the spike domains develop under the influence of a present magnetic field and not during relaxation after the excitation by H_{pulse}. Similar domains are also visible in the investigations on rectangular $Ni_{81}Fe_{19}$ elements ($20 \times 80\ \mu m^2$, 40-nm thick) of Schneider *et al.* in Ref. 24, although they have not been mentioned by the authors. At the top of the element on both sides of the domain with $\vec{M} \| \vec{H}$ spike domains appear similar to our experiments.

The vortex mobility is different in the two examined geometries. In the aligned element (Figs. 5 and 8) the vortex core does not move at all, indicated by the two Néel walls on the right which stay at their positions. This is independent of the size of the element. In the tilted element (Fig. 10), however, the vortex position is shifted by some micrometers perpendicularly to the direction of H_{pulse}. The determining difference lies in the zero initial permeability of the domain oriented parallel to H_{pulse} for the aligned element, whereas all domains respond to the fast rising field in the case of the tilted element. During relaxation in the tilted element, the vortex is slower than the walls moving back into the ground state. As the vortex does not move by itself (it has an effective zero net moment), but the magnetization in the vicinity changes its orientation, domain walls move and "drag" the vortex along. Similar experiments were also reported by Choe *et al.*[23] They studied the response of the vortex state in much smaller $1 \times 1\ \mu m^2$ to $2 \times 1\ \mu m^2$ sized rectangular CoFe elements exposed to 300 ps wide field pulses. In contrast to our investigation, in their experiment the magnetization remains in a Landau-like ground state with a well defined vortex structure. The vortex is just shifted by the pulsed field and rotates around the center of the element. Due to the smaller size of the elements the influence of the stray field at the edges is much stronger than in our experiment. For this reason the magnetization distribution is reorganizing in our case, leading to a much different domain structure in the element, whereas it remains in the Landau state in the case of the small elements. The same is true for another experiment of Park *et al.*,[19] where the excitation field is also small enough to maintain the state of the magnetic domains. The energy pumped into the sample by H_{pulse} dissipates by excitations of spin waves and uniform precession of magnetization. In the experiments reported here the pulsed magnetic field is stronger, which results in the formation of additional domains to reduce the stray field energy. Recently, Kuksov *et al.*[25] reported on the dynamics in permalloy elements of comparable size. The amplitude of the pulsed magnetic field is comparable to our experiments, but the pulse lasts over several nanoseconds. Also the magnetic field excitation is much slower than in our case, leading to different dynamic magnetization behavior. However, their initial domain state is much more complicated. As shown in our article control and adjustment of the initial domain state is very important.

IV. SUMMARY

A technique of time-resolved wide-field Kerr microscopy with ps time resolution based on a pulsed laser light source has been introduced and applied to the investigation of magnetization reversal in square, but differently oriented, permalloy elements. The Landau ground state of the elements has been excited with magnetic field pulses along the element's edge and diagonal, respectively. Depending on the orientation of the element, the magnetization in different domains rotates as the pulse field is applied. To minimize the stray field, which develops during the rotation of magnetization in the center region of the element, compensating spike domains with the initial magnetization component opposite to the pulse field form at the corners of the elements. Due to small uniaxial anisotropy contributions additional domain spreading in the suppositionally zero rf-permeability domains, where the magnetization is aligned antiparallel to the pulse field, are observed. The following relaxation processes are rather slow (lasting over 10 to 15 ns) compared to the formation of the temporary domain structures (about 0.5 ns). The vortex mobility is much lower than the mobility of the 90° domain walls, leading to curved domain walls pinned to the vortex core.

ACKNOWLEDGMENTS

We thank I. Mönch, H. Vinzelberg, C. Krien, R. Kaltofen, and U. Hartmann (all IFW-Dresden) for the sample preparation and R. Hertel (MPI Halle) for the discussion at the DPG spring-meeting 2004. Further thanks go to Time-Bandwidth Products AG and LOT-Oriel GmbH Co KG (especially to R. Siegel) for help during the laser installation. Financial support by the DFG priority program SPP 1133 "Ultrafast Magnetization Processes" is gratefully acknowledged.

*Electronic address: a.neudert@ifw-dresden.de
†Electronic address: j.mccord@ifw-dresden.de

[1] D. O. Smith, J. Appl. Phys. **29**, 264 (1958).
[2] P. Wolf, J. Appl. Phys. **32**, 95S (1961).
[3] R. Conger and G. Moore, J. Appl. Phys. **34**, 1213 (1963).
[4] M. H. Kryder and F. B. Humphrey, J. Appl. Phys. **40**, 2469 (1969).
[5] M. H. Kryder and A. Deutsch, Proc. Soc. Photo-Opt. Instrum. Eng. **94**, 49 (1976).
[6] M. E. Re and M. H. Kryder, J. Appl. Phys. **55**, 2245 (1984).
[7] M. E. Re, D. N. Shenton, and M. H. Kryder, IEEE Trans. Magn. **21**, 1575 (1985).
[8] P. L. Trouilloud, B. E. Argyle, B. Petek, and J. Herman, IEEE Trans. Magn. **25**, 3461 (1989).
[9] M. Kryder, P. Koeppe, and F. Liu, IEEE Trans. Magn. **26**, 2995 (1990).
[10] F. H. Liu, M. D. Schultz, and M. H. Kryder, IEEE Trans. Magn. **26**, 1340 (1990).

[11] M. Freeman and J. Smyth, J. Appl. Phys. **79**, 5898 (1996).
[12] W. Hiebert, A. Stankiewicz, and M. R. Freeman, Phys. Rev. Lett. **79**, 1134 (1997).
[13] C. Back, J. Heidmann, and J. McCord, IEEE Trans. Magn. **35**, 637 (1999).
[14] M. R. Freeman, R. W. Hunt, and G. M. Steeves, Appl. Phys. Lett. **77**, 717 (2000).
[15] Y. Acremann, C. H. Back, M. Buess, O. Portmann, A. Vaterlaus, D. Pescia, and H. Melchior, Science **290**, 492 (2000).
[16] S.-I. Wakana, T. Nagai, and Y. Sakata, J. Magn. Magn. Mater. **235**, 213 (2001).
[17] W. K. Hiebert, L. Lagae, J. Das, J. Bekaert, R. Wirix-Speetjens, and J. D. Boeck, J. Appl. Phys. **93**, 6906 (2003).
[18] M. Buess, R. Höllinger, T. Haug, K. Perzlmaier, U. Krey, D. Pescia, M. Scheinfein, D. Weiss, and C. Back, Phys. Rev. Lett. **93**, 077207 (2004).
[19] J. Park, P. Eames, D. Engebretson, J. Berezovsky, and P. Crowell, Phys. Rev. B **67**, 020403 (2003).
[20] M. Bonfim, G. Ghiringhelli, F. Montaigne, S. Pizzini, N. Brookes, F. Petroff, J. Vogel, J. Camarero, and A. Fontaine, Phys. Rev. Lett. **86**, 3646 (2001).
[21] J. Vogel, W. Kuch, M. Bonfim, J. Camarero, Y. Pennec, F. Offi, F. Fukumoto, J. Kirschner, A. Fontaine, and S. Pizzini, Appl. Phys. Lett. **82**, 2299 (2003).
[22] H. Stoll, A. Puzic, V. van Wayenberge, P. Fischer, J. Raabe, M. Buess, T. Haug, R. Höllinger, C. Back, D. Weiss, and G. Denbeaux, Appl. Phys. Lett. **84**, 3328 (2004).
[23] S.-B. Choe, Y. Acremann, A. Scholl, A. Bauer, A. Doran, J. Stöhr, and H. Padmore, Science **304**, 420 (2004).
[24] C. M. Schneider, A. Kuksov, A. Krasyuk, D. Neeb, S. A. Nepijko, G. Schönhense, I. Mönch, R. Kaltofen, J. Morais, C. de Nadaï, and N. B. Brookes, Appl. Phys. Lett. **85**, 2562 (2004).
[25] A. Kuksov, C. Schneider, A. Oelsner, A. Krasyuk, D. Neeb, G. Schönhense, C. De Nadaï, and N. Brookes, J. Appl. Phys. **95**, 6530 (2004).
[26] A. Hubert and R. Schäfer, *Magnetic Domains* (Springer, Berlin, 1998).
[27] M. Freeman and B. Choi, Science **294**, 1484 (2001).
[28] M. R. Freeman and W. K. Hiebert, *Spin Dynamics of Confined Magnetic Structures I* (Springer, Berlin, 2002), Chap. "Stroboscopic microscopy of magnetic dynamics," pp. 93-126.
[29] B. Argyle and J. McCord, J. Appl. Phys. **87**, 6487 (2000).
[30] D. Chumakov, J. McCord, R. Schäfer, L. Schultz, H. Vinzelberg, R. Kaltofen, and I. Mönch, Phys. Rev. B **71**, 014410 (2005).
[31] H. van den Berg and D. Vatvani, IEEE Trans. Magn. **18**, 880 (1982).
[32] R. Hertel and J. Kirschner, J. Magn. Magn. Mater. **270**, 364 (2004).